Crossover temperatures in the normal-state phase diagram of high-T_c superconductors

G. V. M. Williams and J. L. Tallon
New Zealand Institute for Industrial Research, P.O. Box 31310, Lower Hutt, New Zealand

J. W. Loram
IRC in Superconductivity, Cambridge University, Cambridge CB3 0HE, United Kingdom

(Received 5 January 1998)

The widespread reference to phase diagrams for the high-T_c superconductors that involve two crossover temperatures T_L and T_U extending across the underdoped normal-state region is critically examined in the light of NMR and heat capacity data. We conclude that, in both the $\mathbf{q}=(0,0)$ and $\mathbf{q}=(\pi,\pi)$ response, there is only one crossover temperature, best described as the pseudogap energy scale rather than a well-defined onset temperature. This has a strong, linearly decreasing dependence on hole concentration. The lower crossover temperature, T_L, commonly determined from $^{63}T_1T$, is shown to be an artefact of convoluting the pseudogap energy scale with an intrinsic linear T dependence arising, in the nearly antiferromagnetic Fermi-liquid model, from the characteristic spin-fluctuation frequency, $\omega_{\rm sf}$. We conclude that models constructed on the two-crossover temperatures scenario need to be reexamined. [S0163-1829(98)00338-5]

INTRODUCTION

After 10 years of unprecedented research effort in high-T_c superconductors, there is still no consensus as to the pairing mechanism and the essential physics of the normal state. What is now generally recognized is that for underdoped cuprates there occurs some form of correlation above T_c referred to as the pseudogap state that reduces the electronic entropy, magnetic susceptibility, has a marked effect on transport properties, and is clearly seen in recent angle-resolved photoemission spectroscopy (ARPES) studies on $Bi_2Sr_2CaCu_2O_8$.[1–8] Extensive evidence has now been presented that there is a gap in both spin and charge degrees of freedom.[9] Interpretations of the pseudogap and normal-state properties are manifold, including short-range pairing correlations,[10] formation of real-space pairs,[11] condensation of singlet paired spinons in the spin-charge separation strong-correlation models of Fukuyama, Lee, and their co-workers,[12,13] antiferromagnetic (AF) correlations in the nearly antiferromagnetic Fermi-liquid (NAFL) model,[14] a charge-density wave,[15] charge stripes,[16] and superspin in the SO(5) model of Zhang.[17] All of these models cannot be correct.

Many interpretations of normal-state data above T_c now include two onset temperatures that we label T_L and T_U where the lower, T_L, is variously attributed to the opening of a spin gap,[18] the pseudogap in the normal-state density of states,[14,19] or short-range pairing correlations.[10] T_L has been defined as the position of the peak in $(^{63}T_1T)^{-1}$ (Refs. 20 and 21) or as the temperature at which $^{63}T_1T$ departs from linearity.[22] In the NAFL model, T_L was originally associated with a transition from a quantum critical to a quantum dynamical regime.[23] This model was motivated by the observation of antiferromagnetic correlations in neutron-scattering measurements, although the model requires a temperature-dependent antiferromagnetic correlation length, contrary to analysis of the neutron-scattering data.[24] The NAFL model has now evolved with T_L, becoming the temperature at which the pseudogap opens.[14,22] (We note immediately that this is at odds with heat capacity and tunneling data that show that the pseudogap opens at temperatures much higher than T_L.[9,25] As the proposed T_L is only weakly dependent on hole concentration, the disparity increases with underdoping due to the sharply growing pseudogap energy scale.) An antiferromagnetic-correlation pseudoscaling regime is assumed in the intermediate temperature region where $T_L<T<T_U$, while the upper temperature, T_U, marks the crossover from pseudoscaling to mean-field behavior. It has recently been shown by Corey *et al.*[26] and Curro *et al.*[27] that a T_L and T_U can be deduced from the deviation from linear temperature dependence in $^{63}T_1T/^{63}T_{2G}$ (T_L) and in $^{63}T_1T/^{63}T_{2G}^2$ (T_U) where $^{63}T_{2G}$ is the ^{63}Cu Gaussian spin-spin relaxation time. However, it is acknowledged that there are problems in accurately determining $^{63}T_{2G}$. This quantity is affected by small magnetic fields, the magnitude of the excitation pulse and interactions with neighboring ^{17}O and ^{89}Y nuclei.[27,28] The effect of interactions with unlike neighboring nuclei is more significant at higher temperatures and can obscure the crossover temperature T_U from the data.[29] A crossover temperature is also inferred from transport data,[22,29] infrared data,[30] Raman data[31] and the ARPES leading-edge gap energy[8,32] but this is numerically inconsistent with the T_L obtained from $^{63}T_1T$, having a strong hole concentration dependence.

Clearly, the wide range of models introduced to explain the data as well as the inconsistencies within the interpretation of the data are both unsatisfactory. We address these problems in this paper and make several key points.

(i) We distinguish between an *onset* temperature, such as might be associated with a mean-field transition broadened out due to fluctuations where changes in the spectrum occur over a temperature range small in comparison with T, and an *energy scale* where changes take place over a broad temperature range comparable with T and are thus determined by a single and at most, weakly T dependent, energy scale. In the terminology we adopt here, an energy scale may be loosely

described as having an associated *crossover* temperature[10] but not an *onset* temperature.

(ii) There are no well-defined ''kinks'' in the normal-state NMR, thermodynamic, and transport data at well-defined onset temperatures, T_L or T_U, as is widely suggested. Careful measurements and analysis of these properties shows a smooth evolution with temperature revealing a single underlying energy scale that can be accurately characterized.

(iii) The subdivision of the normal-state phase diagram by two onset temperatures and the complex scenarios constructed on this assumption is not supported by a careful analysis of the NMR, heat capacity, and transport data. In particular, we take issue with the inference, from $1/^{63}T_1T$, of a separate lower T_L associated with the opening of a spin gap.

(iv) The pseudogap is present equally in both spin and charge degrees of freedom. Moreover, the pseudogap is present equally in the $\mathbf{q}=(0,0)$ and $\mathbf{q}=(\pi,\pi)$ response as confirmed by the Knight shift, $^{63}T_1^{-1}$ and electronic entropy, $S_{\rm el}$. Put another way, the pseudogap and the spin gap are one and the same.

(v) While the above key points are quite general and independent of the NAFL model, we show that they can be quantitatively accounted for within the NAFL model if the magnitude of the peak in the dynamical spin susceptibility at $\mathbf{q}=(\pi,\pi)$ varies as $\chi_s\xi^2$ where χ_s is the static spin susceptibility and ξ is the antiferromagnetic correlation length, as originally proposed by Millis, Monien, and Pines.[33]

EXPERIMENTAL DETAILS

Phase-pure polycrystalline samples of $YBa_2Cu_4O_8$ were synthesized by standard solid-state reaction at 945 °C and 60 bar oxygen pressure. $Y_{1-x}Ca_xBa_2Cu_3O_{7-\delta}$ samples were synthesized by initially decomposing a stoichiometric mixture of Y_2O_3, $Ca(NO_3)_2$, $Ba(NO_3)_2$, and CuO in air at 700 °C for 1 h. This was followed by reactions in air at 900 °C for 6 h and 915, 930, 940, and 950 °C for 24 h. The samples were then heated at 980 °C in O_2 at 1 bar for 6 h followed by rapid cooling to 350 °C and then at 350 °C for 48 h to achieve maximum overdoping. The samples were reground after each sinter. The hole concentrations were varied by annealing in nitrogen/oxygen gas mixtures at a variety of oxygen partial pressures and temperatures. X-ray-diffraction analysis showed that the samples were single phase and there was no evidence of the $Ba_4CaCu_3O_8$ and $BaCuO_2$ impurity phases that are known to occur when there is partial Ca substitution of Ba.

ac susceptibility measurements were used to determine the T_c values. The hole concentration p was determined from thermoelectric power[34] and from the relation $T_c/T_{c,\rm Max}=1-82.6(p-0.16)^2$.[35]

Variable-temperature ^{89}Y NMR measurements were performed at temperatures between 120 and 370 K using a Doty Super-VT Penguin probe, a Varian Unity 500 spectrometer, and a 11.74 T superconducting magnet. Magic-angle spinning MAS at a frequency of ~2.5 kHz was used to remove dipole-dipole coupling and dramatically reduce the spectral linewidth. The narrow $YBa_2Cu_4O_8$ ^{89}Y NMR MAS linewidth (~100 Hz at 293 K) coupled with long acquisition times and accurate temperature control enabled high accuracy in the temperature-dependent NMR shifts to be obtained. The spectra were collected using the 90-τ-180 spin-echo technique where τ was set to one rotor period and the NMR shifts were referenced to a 1 molar aqueous solution of YCl_3.

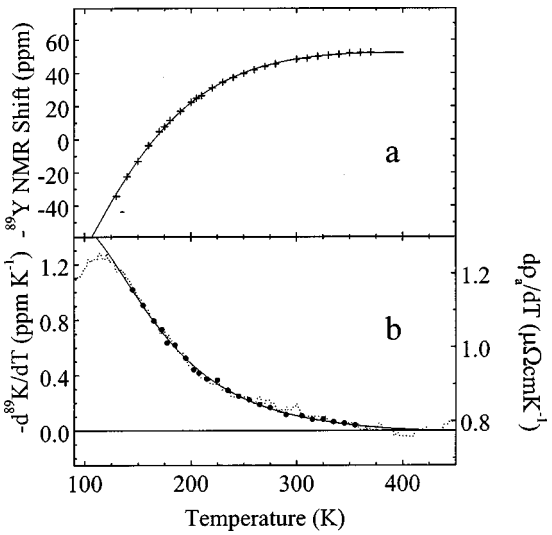

FIG. 1. (a) Plot of the MAS ^{89}Y NMR shift from a $YBa_2Cu_4O_8$ sample (+). The solid curve is a fit to the data using the model described in the text. (b) Plot of the derivative of the NMR shift data (solid circles) and the solid curve in (a). Also shown by the dotted curve is $\partial\rho_a/\partial T$ as a function of temperature from resistivity measurements on a $YBa_2Cu_4O_8$ single crystal where ρ_a is the electrical resistivity in the a direction (Ref. 36).

RESULTS AND ANALYSIS

The first point we wish to make is that no onset temperature is apparent in the NMR shift, transport, and thermodynamic data, i.e., there is no temperature, or narrow range of temperatures, in which the character of the spectrum significantly alters resulting in the ''kinks'' widely claimed to be present in these properties. This is apparent in Fig. 1(a) where we plot high-precision variable-temperature MAS ^{89}Y NMR shift data from a $YBa_2Cu_4O_8$ sample. The NMR shift is proportional to the static spin susceptibility and can be expressed as[33]

$$K=\frac{\sum_j A_j}{\gamma_n\gamma_e\hbar^2}\chi_s+\sigma, \tag{1}$$

where A_j are the hyperfine coupling constants (negative for ^{89}Y), γ_n is the nuclear gyromagnetic ratio, γ_e is the electron gyromagnetic ratio, χ_s is the static spin susceptibility and σ is the temperature-independent chemical shift. The first term is the Knight shift, K_s. The low noise in the ^{89}Y NMR shift data is evident in Fig. 1(b) where we plot the temperature derivative of the ^{89}Y NMR shift. From Eq. (1) it is apparent that $d^{89}K/dT$ is directly proportional to $d\chi_s/dT$. This progresses smoothly and asymptotically towards zero at high temperature. The derivative is very sensitive to kinks in the original data and nowhere does the derivative fall suddenly so as to signal an onset or transition. No features can be

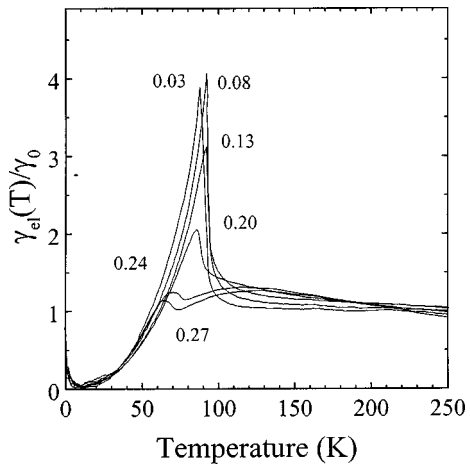

FIG. 2. (a) Plot of the normalized γ_{el} against temperature for $YBa_2Cu_3O_{7-\delta}$ samples with δ values shown (Ref. 37). Note that optimal doping corresponds to $\delta \sim 0.1$.

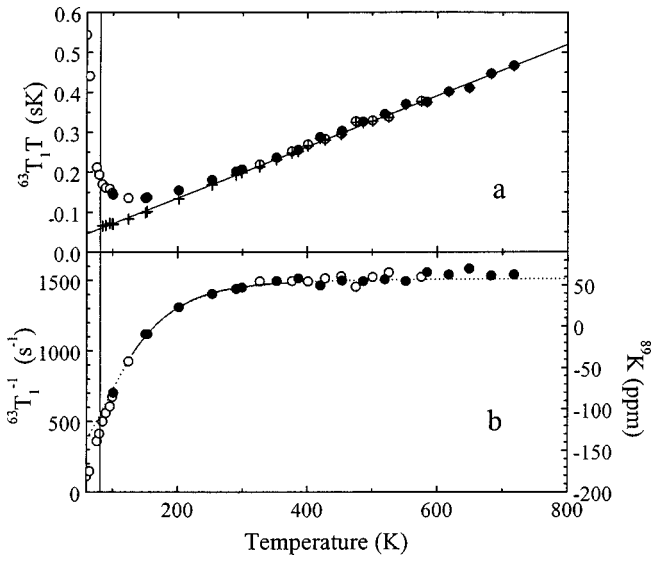

FIG. 3. (a) Plot of $^{63}T_1T$ against temperature (open and solid circles) and $^{63}T_1T^{89}K_s(T)/^{89}K_s(\infty)$ against temperature (+) for a $YBa_2Cu_4O_8$ sample where $^{89}K_s(T)$ was obtained from the best fit to the data in Fig. 1(a). The $^{63}T_1T$ data is from Curro *et al.* (○) (Ref. 27) and Corey *et al.* (●) (Ref. 26). The solid vertical line indicates T_c. (b) Plot of $(^{63}T_1)^{-1}$ against temperature using the data plotted in (a). Also included is the ^{89}Y NMR data (solid curve) and best fit curve (dotted curve) from Fig. 1(a). The solid vertical line indicates T_c.

observed near 160 K (Ref. 20) or 215 K (Ref. 27) where crossover temperatures have previously been deduced for $YBa_2Cu_4O_8$. Similarly, the normal-state thermodynamic functions $\gamma_{el}=C_{el}/T$ and S_{el}/T where S_{el} is the electronic entropy have a smooth broad temperature evolution, free of any apparent onsets indicated by an accelerated change in slope. The absence of any apparent onset temperatures above T_c in the heat capacity is evident in Fig. 2 where we plot γ_{el} for underdoped to slightly overdoped $YBa_2Cu_3O_{7-\delta}$ samples.[9]

The absence of a well-defined crossover temperature has also been noted by Hussey *et al.*[36] from resistivity measurements on high-quality $YBa_2Cu_4O_8$ single crystals. We plot the derivative of their data, $d\rho_a/dT$, in Fig. 1(b) where the smooth temperature evolution over the entire temperature range is again apparent. The result is remarkably similar to the derivative of the ^{89}Y Knight shift. Where T_L values have previously been determined from resistivity data, it has been done so by a linear extrapolation of the high-temperature data and defining T_L as the temperature at which significant deviation from linearity is observed. Such a method ''by eye'' is deceptive because the data convolutes a linear temperature term with another that has the characteristic pseudogap temperature dependence giving the appearance of a sudden downturn that simply is not there as shown by the $d\rho_a/dT$ data. Specifically, the resistivity may be written, $\rho=\rho_0+g(T)bT$ where $g(T)$ is function between 0 and 1 that accounts for the normal-state pseudogap, ρ_0 is the residual resistivity, and b is the high-temperature expansion linear temperature coefficient.

Although many different constructions have been placed on the supposed onset temperatures they all incorporate the idea of a change in the character of the electronic and/or spin spectrum occurring at or around some temperature as, e.g., in a mean-field transition that is broadened out due to fluctuations. The data in Figs. 1 and 2 forces us to conclude that *the normal-state spectrum is characterized by an energy scale and not a temperature scale*. The clear distinction is that, for the former, all derivatives change smoothly with temperature with peaks in higher derivatives progressing to lower temperature. In contrast, a temperature scale as for the onset of an order parameter shows pronounced features in all derivatives occurring around the same critical temperatures, T_L or T_U. The specific heat is particularly valuable in establishing the nonexistence of onset temperatures since it reflects the energy dependence of both the spin and charge excitations over all values of **q**. It is very sensitive to abrupt changes as evidenced by the large jump in γ_{el} at T_c, seen in Fig. 2, due to the onset of superconductivity. We stress the absence of anomalies in γ_{el} at expected values of T_L or T_U for a wide range of underdoped cuprates [$YBa_2Cu_3O_{7-\delta}$, $YBa_2Cu_4O_8$, $La_{2-x}Sr_xCuO_4$, $Tl_{0.5}Pb_{0.5}-1212$, and $Tl_2Ba_2Ca_2Cu_3O_{10}$ (Ref. 37)] indicating that *there are no obvious onset temperatures in either the charge or spin spectrum.*

Having shown above that there are no onset temperatures in the resistivity, the $\mathbf{q}=(0,0)$ response of the NMR shift, and the summed response for all **q** in γ_{el}, we turn to the ^{63}Cu spin-lattice relaxation data from which a T_L has been deduced. As noted above, this T_L is generally associated with the opening of a spin gap[21] and is given by the position of the peak observed in $(^{63}T_1T)^{-1}$ or the temperature at which $^{63}T_1T$ departs from linearity, as can be seen in Fig. 3(a) where we plot the $^{63}T_1T$ data of Curro *et al.* (filled circles) (Ref. 27) and Corey *et al.* (open circles) (Ref. 26) against temperature for $YBa_2Cu_4O_8$. However, we show in Fig. 3(b) where $^{63}T_1^{-1}$ (circles) and ^{89}K (solid curve) are plotted against temperature, that $^{63}T_1^{-1}$ is directly proportional to ^{89}K with $^{89}\sigma=200$ ppm. This means that $^{63}T_1^{-1}$ has the same single underlying energy scale that $^{89}K_s$ has and the appearance of an onset temperature, T_L originates from the division of $^{63}T_1^{-1}$ by T. This is apparent in Fig. 3(a) where we plot $^{63}T_1T^{89}K_s(T)/^{89}K_s(\infty)$ (crosses) where $^{89}K_s(T)$ is the ^{89}Y Knight shift and $^{89}K_s(\infty)$ is the high-temperature

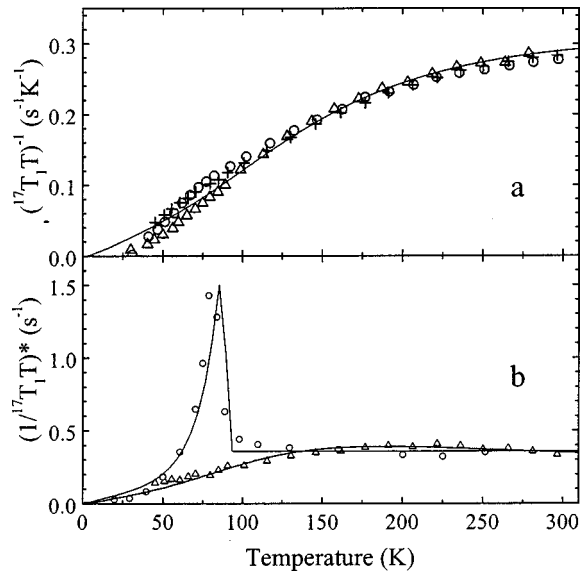

FIG. 4. (a) Plot of $(^{17}T_1T)^{-1}$ (+) against temperature for $YBa_2Cu_3O_{6.63}$ (Ref. 38). Also included is $(^{63}T_1)^{-1}$ (○) (Ref. 38) and $^{17}K_s$ (△) (Ref. 38) for the same sample and scaled so as to coincide with the $(^{17}T_1T)^{-1}$ data. (b) Plot of $(1/^{17}T_1T)^* = (d/dT)$ $(^{17}T_1^{-1})$ against temperature for $YBa_2Cu_3O_{6.63}$ (△) and $YBa_2Cu_3O_7$ (○) using the data of Takagawa *et al.* (Ref. 38). The solid curves are fits to the data using the model described in the text.

^{89}Y Knight shift. We use our high precision $^{89}K_s$ data extended to higher temperatures using the model described later [solid curve in Fig. 1(a)]. The result is exceptionally linear over the entire temperature range having no feature at a T_L of 160 K (Ref. 20) or 215 K.[27] It should be noted that this observation is substantially model-independent based, as it is, on our experimental Knight-shift data between 130 and 370 K. The model only effects the extremities in Fig. 3(a).

In this regard, a key observation by Takigawa *et al.*[38] has largely been ignored. They showed that the ratio $^{17}T_1/^{63}T_1$ is quite featureless at the T_L observed in $(^{63}T_1T)^{-1}$. These authors noted ''this suggests a possibility that the peak in $(^{63}T_1T)^{-1}$ is a combined effect of the T dependence of $\chi_{\rm spin}$ and the development of AF correlations and may not require a spin gap opening around 150 K.'' The same result was obtained by Tomeno *et al.*[20] in the case of $YBa_2Cu_4O_8$. It is a consequence of $^{63}T_1^{-1}$ and $(^{17}T_1T)^{-1}$ having the same temperature dependence as ^{17}K as shown in Fig. 4(a) where we plot the $^{63}T_1^{-1}$, $(^{17}T_1T)^{-1}$, and ^{17}K data of Takigawa *et al.* for $YBa_2Cu_3O_{6.63}$.[38] Furthermore, we show by the solid curve that ^{17}K, above T_c, can be well described by the χ_s scaling curve discussed later.

To understand the importance of these observations, we note that in a single-spin component picture $(T_1T)^{-1}$ can be written quite generally as[23]

$$(T_1T)^{-1}=\frac{k_B}{2\mu_B^2\hbar^2}\sum_{\mathbf{q}}|A(\mathbf{q})|^2\,\frac{\chi''(\mathbf{q},\omega)}{\omega}, \qquad (2)$$

where $|A(\mathbf{q})|$ is the form factor expressed as $A(\mathbf{q}) = \Sigma_j A_j \exp(i\mathbf{q}\cdot\mathbf{r}_j)$, A_j are hyperfine coupling constants, μ_B is the Bohr magneton, and $\chi''(\mathbf{q},\omega)$ is the imaginary part of the dynamic spin susceptibility. For a metal, it can be shown that Eq. (2) reduces to the Korringa relation, $(T_1T)^{-1}\propto K_s^2$. However it is apparent in Fig. 4(a) that the Korringa relation is not satisfied since $(^{17}T_1T)^{-1}\propto {}^{17}K_s$ and $(^{63}T_1T)^{-1} \propto {}^{17}K_s/T$ implying a **q**-dependent dynamic susceptibility consistent with the antiferromagnetic spin correlations observed in neutron-scattering measurements. The Mila-Rice Hamiltonian[39] can be used to determine the **q** dependence of the form factor in Eq. (2) leading to $(^{63}T_1T)^{-1}$ being strongly weighted by $\chi''(\mathbf{q},\omega)$ near the antiferromagnetic wave vector, $\mathbf{q}=(\pi,\pi)$ and $(^{17}T_1T)^{-1}$ strongly weighted by **q** near $\mathbf{q}=(0,0)$.[33] Thus the observation that $(^{17}T_1T)^{-1} \propto {}^{17}K_s$ and $(^{63}T_1T)^{-1}\propto {}^{17}K_s/T$ implies that the normal-state pseudogap exists in the entire spin spectrum and not just near $\mathbf{q}=(0,0)$. This conclusion is consistent with the analysis of $S_{\rm el}$ and χ_sT by Loram *et al.*[9] who showed that $\chi_sT/S_{\rm el}$ is close to the Wilson ratio, a_w, for weakly interacting Fermions and that the normal-state pseudogap exists equally in the charge and spin degrees of freedom. It is important to emphasize, therefore, that *the pseudogap is not a spin gap only*.

The experimentally observed correspondence between $S_{\rm el}$ and $a_w\chi_sT$ over a wide range of temperatures for several cuprate systems provides convincing evidence that the magnitude and T dependence of χ_s is dominated by the (energy-dependent) single-particle density of states. In this circumstance both χ_sT and $S_{\rm el}$ directly count the number of quasiparticle states within the Fermi window. Because of this there is a similar correspondence between $\gamma_{\rm el}=\partial S_{\rm el}/\partial T$ and $\chi^*=(d/dT)(\chi_sT)$, viz. $\gamma=a_w\chi^*$. Moreover, because $(^{17}T_1T)^{-1}\propto\chi_s$, then a similar correspondence should exist between $\gamma_{\rm el}$ and $(1/^{17}T_1T)^*=(d/dT)(^{17}T_1^{-1})$. This is exploited in Fig. 4(b) that shows the temperature dependence of $(1/^{17}T_1T)^*$ for two different doping states of $YBa_2Cu_3O_{7-\delta}$, one with $\delta\sim 0$ where there is no pseudogap and the other with $\delta\sim 0.37$ and a large pseudogap energy. A strong resemblance is seen to the data for $\gamma_{\rm el}$ plotted in Fig. 2 that will be discussed later, including the broad enhancement above T_c in the underdoped sample and the dramatic suppression of the jump occurring at T_c when the pseudogap appears. The solid curves are calculated using the model discussed later. (*We have intentionally left the issue of modelling to the end of this paper because we wish to emphasize that the foregoing analysis and conclusions are essentially model independent.*)

We have shown above that there are no onset temperatures in the normal-state NMR, transport, and thermodynamic data consistent with our previous analysis showing that the data are much better described by an energy scale. This is apparent in Fig. 5 where we show the normalized ^{89}Y NMR shift, $^{89}K_n(T)$ for a wide range of doping states for (a) $Y_{0.9}Ca_{0.1}Ba_2Cu_3O_{7-\delta}$ and (b) $Y_{0.8}Ca_{0.2}Ba_2Cu_3O_{7-\delta}$ plotted against a scaling parameter $z=2k_BT/E_g$ where E_g is the pseudogap energy. $^{89}K_n(T)$ was determined from $^{89}K_n(T) = [^{89}K(T)-{}^{89}K(0)]/[^{89}K(\infty)-{}^{89}K(0)]$ where $^{89}K(\infty)$ is $^{89}K(T)$ at high temperatures and $^{89}K(0)$ is $^{89}K(T)$ at $T=0$ K. It can be seen that, in spite of the wide range of doping, the data closely follow the scaling curve to be described later and in general terms it is evident that there is an underlying energy scale without the appearance of onset temperatures. This is more apparent in the superconducting phase diagram for $Y_{1-x}Ca_xBa_2Cu_3O_{7-\delta}$ (Ref. 40) plotted in

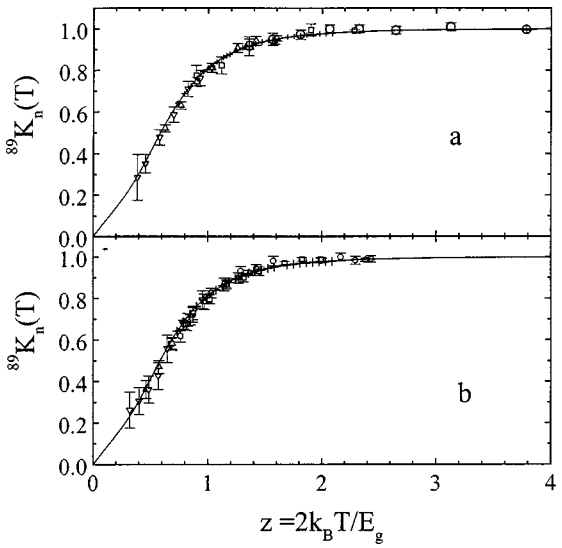

FIG. 5. (a) Plot of the scaled ^{89}Y NMR shift, $^{89}K_n(T)$, against scaling parameter, $z=2k_BT/E_g$, for $Y_{0.8}Ca_{0.2}Ba_2Cu_3O_{7-\delta}$ with T_c and p values of 86 K, $p=0.173$ (○) 83.2 K, $p=0.136$ (□) 65.8 K, $p=0.105$ (△) and 47.5 K, $p=0.086$ (▽). (b) Plot of the scaled ^{89}Y NMR shift, $^{89}K_n(T)$, against scaling parameter, $z=2k_BT/E_g$, for $Y_{0.9}Ca_{0.1}Ba_2Cu_3O_{7-\delta}$ with T_c and hole concentration, p, values of 84.9 K, $p=0.135$ (○), 65 K, $p=0.099$ (□), 57 K, $p=0.082$ (△) and <4 K, $p=0.053$ (▽). The solid curves in (a) and (b) are the scaling curve described in the text.

Fig. 6 where we show the p dependence of T_c (solid curve) and the energy scale, E_g (open symbols), obtained from the scaling operation that generated the data in Fig. 5. Also included is E_g determined from heat capacity measurements on $Y_{0.8}Ca_{0.2}Ba_2Cu_3O_{7-\delta}$. It can be seen that there is a clear correspondence between E_g from χ_s that measures the $\mathbf{q}=(0,0)$ response and from $S_{\rm el}$ that averages over all values of $\mathbf{q}$, further affirming that the normal-state pseudogap exists in both the spin and charge degrees of freedom and across all $\mathbf{q}$. Moreover, E_g is seen to grow with underdoping towards the magnitude of $J\sim 1200$ K, far too high for the pseudogap

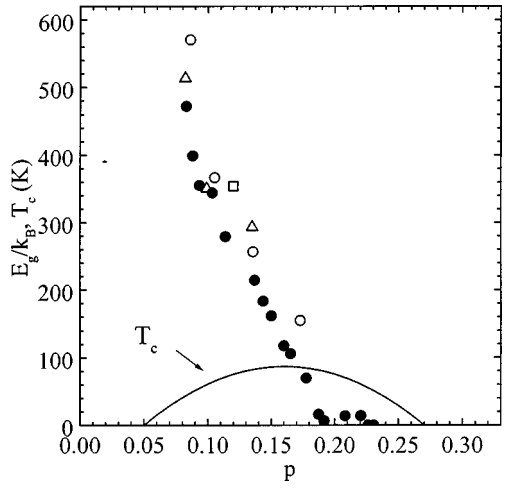

FIG. 6. Plot of the hole concentration dependence of T_c (solid curve), E_g determined from the scaling of the ^{89}Y NMR data for $Y_{0.9}Ca_{0.1}Ba_2Cu_3O_{7-\delta}$ (△), $Y_{0.8}Ca_{0.2}Ba_2Cu_3O_{7-\delta}$ (○), and $YBa_2Cu_4O_8$ (□) and E_g determined from the heat capacity data for $Y_{0.8}Ca_{0.2}Ba_2Cu_3O_{7-\delta}$ (●) (Ref. 40).

to be associated with short-range Cooper pair correlations. Evidently, it is T_U that is to be identified with the energy scale of E_g. As the supposed lower T_L is considered to have but a weak p dependence then, for each different hole concentration represented in Figs. 5(a) and 5(b), T_L would correspond to a different value of $z=2k_BT_L/E_g$. The fact that the data for all hole concentrations lie on the same universal curve means that it is free of any anomalies that might be associated with a T_L.

In the NAFL model the depression in the Knight shift for $T_L<T<T_U$ is attributed to growing antiferromagnetic correlations and for $T<T_L$ there is an abrupt opening of a pseudogap that is temperature independent below T_L.[14] We have seen that (i) T_L has no basis in the $(^{63}T_1T)^{-1}$ data, (ii) T_U can only be considered as an energy scale, and (iii) that χ_s is not reduced due to the freezing out of spin degrees of freedom only but due to freezing out or loss of spectral weight in the total spin and charge system. The correlations giving rise to the pseudogap cannot therefore just be antiferromagnetic spin fluctuations. However, none of the features listed above are essential components of the NAFL model as originally proposed. We consider this model in more detail below.

In the NAFL model, $^{63}T_1T$ is proportional to the characteristic spin-fluctuation frequency $\omega_{\rm sf}$, where the departure of $\omega_{\rm sf}$ from linearity is assumed to originate from the opening of the pseudogap. We show below that $^{63}T_1T$ can be modeled within the NAFL model by a linear temperature dependence in $\omega_{\rm sf}$ that remains linear in spite of the opening of the pseudogap. Millis, Monien, and Pines[33] have developed a phenomenological dynamical spin susceptibility that is expressed by Pines[19] in the NAFL model as

$$\chi(\mathbf{q},\omega)=\frac{\beta\xi^2}{[1+(\mathbf{Q}-\mathbf{q})^2\xi^2-i\omega/\omega_{\rm sf}]}+\frac{\chi_s(T)}{1-i\omega/\Gamma_0}, \quad (3)$$

where ξ is the antiferromagnetic correlation length ratioed by the in-plane lattice parameter, $\omega_{\rm sf}$ is the paramagnon frequency, $\chi_s(T)$ is the temperature-dependent static spin susceptibility, and Γ_0 is the temperature-independent effective bandwidth. The first term accounts for the strong antiferromagnetic correlations about $\mathbf{Q}=(\pi,\pi)$ while the second term is the Fermi-liquid term. However, this phenomenological dynamical spin susceptibility with a temperature-independent β seems to imply the existence of a gap near $\mathbf{q}=(0,0)$ and none near $\mathbf{q}=(\pi,\pi)$. This is inconsistent with the scaling of χ_s and $S_{\rm el}/T$ mentioned earlier which clearly shows that the pseudogap is in both the spin and charge degrees of freedom.[9] Furthermore, inserting Eq. (3) into Eq. (2) will not lead to the experimental observation that $(^{17}T_1T)^{-1}\propto\chi_s$ and $(^{63}T_1T)^{-1}\propto\chi_s/T$ as evidenced by Figs. 3 and 4. However, this can easily be rectified by writing $\beta=a_0\chi_s(T)$ as originally proposed by Millis, Monien, and Pines where a_0 is a constant.

Inserting Eq. (3) into Eq. (2), using the Mila-Rice Hamiltonian and $\beta=a_0\chi_s(T)$ leads to $(^{63}T_1T)=a_1\omega_{\rm sf}/\chi_s(T)$ and $(^{17}T_1T)=a_2\Gamma_0/\chi_s(T)$ in the limit of $\xi\gg 1$ where a_1 and a_2 are constants. Thus $(^{17}T_1T)\chi_s(T)=a_2\Gamma_0$ and $(^{63}T_1T)\chi_s=a_1\omega_{\rm sf}$. Consequently, all the features of Figs. 3 and 4 are recovered and, in particular, it can be seen in Fig. 3 (crosses)

that $\omega_{sf}(=^{63}T_1T\chi_s)$ is precisely linear in temperature and lacking any feature that might indicate the appearance of a T_L or T_U in the normal state.

Crossover or onset temperatures have also been deduced from the ^{63}Cu Gaussian spin-spin relaxation time $^{63}T_{2G}$ within the NAFL model with a temperature-independent β.[27] This was interpreted as arising from the relation $\omega_{sf}\xi$ = constant in a pseudoscaling temperature region, $T_L<T<T_U$ and $\omega_{sf}\xi^2$ = const in a mean-field temperature region, $T>T_U$, where $T_L\approx 200$ K and $T_U\approx 500$ K. When $T<T_L$, it is assumed that ω_{sf} increases with decreasing temperature due to the opening of the pseudogap. However, the inclusion of $\beta=a_0\chi_s(T)$ to account for the experimental data in Figs. 3 and 4 leads to an ω_{sf} that is linearly dependent on temperature without any evidence of an onset temperature near 200 K. We show below that the apparent onset temperatures are due to the temperature dependence of ξ^{-1}.

We start with an expression that has been derived for $^{63}T_{2G}$,[23]

$$^{63}T_{2G}^{-2}=\left(\frac{0.69}{128}\right)^{0.5}(^{63}\gamma_n)^2\left[\frac{1}{N}\sum_{\mathbf{q}}|^{63}A_{\rm eff}(\mathbf{q})|^4\chi'(\mathbf{q},0)^2-\left(\frac{1}{N}\sum_{\mathbf{q}}|^{63}A_{\rm eff}(\mathbf{q},\omega)|^2\chi'(\mathbf{q},0)\right)^2\right], \tag{4}$$

where $^{63}A_{\rm eff}(\mathbf{q})$ is the effective ^{63}Cu form factor and $^{63}\gamma_n$ is the ^{63}Cu nuclear gyromagnetic ratio. Using the Mila-Rice Hamiltonian, Eq. (3), and the limit $\xi\gg 1$, it can be shown that $^{63}T_{2G}^{-1}=a_3\chi_s(T)\xi$. Thus,

$$\frac{^{63}T_1T}{^{63}T_{2G}}=a_1a_3\omega_{sf}\xi \tag{5}$$

and

$$\frac{^{63}T_1T}{^{63}T_{2G}^2}=a_1a_3^2\chi_s(T)\omega_{sf}\xi^2. \tag{6}$$

It has been observed experimentally that $^{63}T_1T/^{63}T_{2G}$ is approximately constant for 200 K$\lesssim T\lesssim$500 K and $^{63}T_1T/^{63}T_{2G}^2$ is approximately constant for $T>500$ K, leading to the pseudogap, pseudoscaling, and mean-field temperature regions discussed above.[26,27] However, when $\beta=a_0\chi_s(T)$, then

$$\xi^{-1}=a_3\chi_s(T)^{63}T_{2G}. \tag{7}$$

In Fig. 7 we show ξ^{-1} plotted against temperature where $\chi_s(T)$ in Eq. (7) is obtained from the scaling curve in Fig. 5 and $^{63}T_{2G}$ was obtained from the data of Curro *et al.*[27] It can be seen that ξ^{-1} decreases monotonically with decreasing temperature but unlike $\omega_{sf}(=^{63}T_1T\chi_s)$ plotted in Fig. 3(a) it is not linearly dependent on temperature over the entire range. In Fig. 8 we show (a) $\omega_{sf}\xi$ and (b) $\omega_{sf}\xi^2$ plotted against temperature using $\omega_{sf}(T)$ plotted in Fig. 3(a) and $\xi^{-1}(T)$ plotted in Fig. 7. *If it is to be argued that* $\omega_{sf}\xi$ is approximately constant for 150 K$\lesssim T\lesssim$500 K and $\omega_{sf}\xi$ is approximately constant for $T\gtrsim 500$ K (*although the solid curves as guides to the eye, would suggest this is over interpreting the data*), then it is apparent from Figs. 7 and 3(a) that this ''scaling'' arises solely from the temperature dependence of $\xi^{-1}(T)$ where $\xi^{-1}(T)$ is approximately proportional to T in the intermediate temperature region and approximately proportional to $\sqrt{T}$ in the high-temperature region.

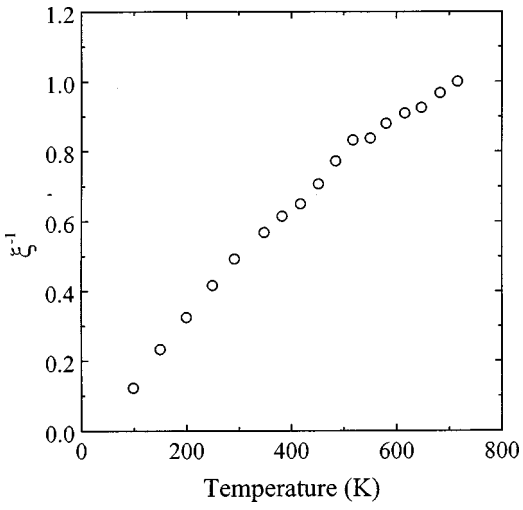

FIG. 7. Plot of the $YBa_2Cu_4O_8$ inverse antiferromagnetic correlation length ξ^{-1} against temperature as obtained from $\chi_s(T)$ and $^{63}T_{2G}$ using Eq. (7) where ξ^{-1} is normalized to the value at the highest temperature. The $\chi_s(T)$ data were obtained from the best fit to the data in Fig. 1(a) and the $^{63}T_{2G}$ data are from Curro *et al.* (Ref. 27).

We now turn to modeling the temperature dependence of the NMR shift and thermodynamic data. We have previously shown that the NMR Knight-shift data can be modeled by a temperature-independent normal-state gap with *d*-wave-like symmetry and without the inclusion of onset temperatures.[5,41,42] We used the model of Loram *et al.*[1] where the quasiparticle energy is written as $E(\mathbf{k})=[\varepsilon(\mathbf{k})^2+\Delta(\mathbf{k})^2]^{1/2}$ with $\Delta(\mathbf{k})^2$ being $\Delta(\mathbf{k})^2=\Delta'(\mathbf{k})^2+E_g(\mathbf{k})^2$ where $\Delta'(\mathbf{k})$ is the superconducting order parameter (zero above T_c) and $E_g(\mathbf{k})$ is the normal-state pseudogap energy. This model has proved successful in accounting for the decrease in condensate energy[40] with increased underdoping, the p dependence of the jump in the heat capacity at T_c (Ref.

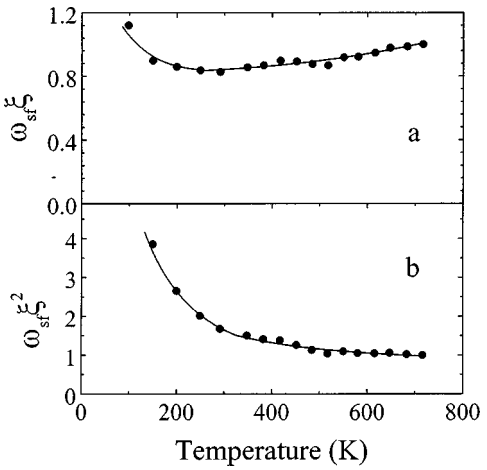

FIG. 8. Plot of (a) $\omega_{sf}\xi$ and (b) $\omega_{sf}\xi^2$ against temperature from the plots in Figs. 3(a) and 7. The data were scaled to the high-temperature value. The lines are guides to the eye.

1) and the p dependence of the T_c suppression by Ni or Zn impurities.[43,44] While this model adopts a specific dispersion, its success lies in the fact that it generally reflects the impact on superconducting properties of lost spectral weight due to the presence of the pseudogap. We proceed with this model here in this spirit and do not wish to suggest that our approach is limited to a particular dispersion. Almost indentical results are obtained for a nonstates conserving triangular gap in the density of states (DOS) and are therefore not critically dependent on the specific model. The key benefits that we derive from this modeling is that it provides a basis for understanding the scaling behavior to which we have referred and a means to extrapolate the observed behavior in χ_s to high or low temperatures for comparison with $1/T_1T$ data.

As shown in Eq. (1), $^{89}K_s$ is proportional to χ_s and we have previously modeled χ_s using the Pauli spin susceptibility,

$$\chi_s = \mu_B^2 \int_{-\infty}^{\infty} N(E)\left(-\frac{\partial f}{\partial E}\right) dE, \tag{8}$$

where $N(E)$ is the density of states and $f(E)$ is the Fermi function. Similarly, the electronic entropy may be expressed as

$$S_{\rm el} = -k_B \int_{-\infty}^{\infty} N(E)\{f(E)\ln[F(E)] + [1-f(E)]\ln[1-f(E)]\} dE. \tag{9}$$

As noted above, this procedure is justified by the observed correspondence between $S_{\rm el}$ and $a_w\chi_s T$ that emerges from Eqs. (8) and (9) because the specific Fermi windows are almost identical. Using these relations, the NMR, susceptibility, and thermodynamic data have been successfully modeled using a d-wave superconducting order parameter expressed as $\Delta'(\mathbf{k}) = \Delta' \cos(2\phi)$ and a d-wave-like normal-state pseudogap expressed as $E_g(\mathbf{k}) = E_g|\cos(2\phi)|$ (Ref. 40) consistent with recent ARPES data. The two-dimensional density of states was obtained from the quasiparticle energy dispersion, $E(\mathbf{k}) = [\varepsilon(\mathbf{k})^2 + E_g(\mathbf{k})^2 + \Delta'(\mathbf{k})^2]^{1/2}$ with $\varepsilon(\mathbf{k}) = \hbar^2k^2/2m^*$ where m^* is the effective mass. This form for $\varepsilon(\mathbf{k})$, leading to a cylindrical Fermi surface, is used because it conveniently leads to $N(E)$ being simply expressed in terms of an elliptic integral. We note that ARPES measurements on optimally doped and overdoped samples where E_g is small indicate that the Fermi surface is not cylindrical and some studies also indicate a shadow Fermi surface.[45] Various energy dispersions have been derived from the k dependence of the Fermi surface.[19,46] The situation is complicated by recent ARPES measurements on underdoped $Bi_2Sr_2CaCu_2O_{8-\delta}$ that indicate the absence of quasiparticle peaks in the ARPES spectra above T_c and near $\mathbf{k} = (\pm\pi, 0)$ and $\mathbf{k} = (0, \pm\pi)$, the very regions in k space where E_g is at a maximum.[47] Interpretations of this behavior include collective excitations leading to a significant reduction in quasiparticle lifetimes with the possibility of a non-Fermi liquid in this region,[48] or strong interactions with collective excitations that lead to a decrease in spectral weight at the quasiparticle peak in the ARPES spectra.[47] We note that the model of Loram *et al.*[1] is still valid near T_c because the states near the zone boundary contribute little to the thermodynamic, magnetic, or transport properties owing to the magnitude of E_g.

Given the various interpretations of the ARPES data and the different dispersion relations used, we retain $\varepsilon(\mathbf{k}) = \hbar^2k^2/2m^*$. We note that when the Fermi energy, E_F, is sufficiently removed from half filling this form of the energy dispersion is a good approximation. It is also possible to account for the absence of quasiparticle peaks near $\mathbf{k} = (\pm\pi, 0)$ and $\mathbf{k} = (0, \pm\pi)$, by not including these states in calculating the density of states while using a tight-binding energy dispersion with the Fermi level lying near the saddle point. This can lead to a flat density of states near the Fermi level. The important point, as seen in the low-temperature thermodynamic data and the NMR data plotted in Fig. 4, is that, for the underdoped $Y_{1-x}Ca_xBa_2Cu_3O_{7-\delta}$ compounds, $N(E)$ is linear near E_F and $N(E)$ is such that at high temperatures χ_s is constant. We account for the Fermi-surface evolution observed in a recent ARPES study[49] by setting $E_g(\mathbf{k}) = E_g[|\cos(2\phi)| - F(z)]/[1 - F(z)]$ where $F(z) = 1 - \tanh^N(z)$ and $z = E_g/2k_BT$. This functional form for E_g allows $E_g(\mathbf{k})$ to equal $E_g|\cos(2\phi)|$ at low temperatures and for the Fermi surface to be completely recovered at high temperatures, as observed. It directly leads to a filling in of the pseudogap density of states. We show in Figs. 1(a), 4, and 5 that the resultant χ_s scaling curve can very satisfactorily describe the data (solid curves) with $N = 4$. This Fermi-surface evolution model also accounts for the decrease in the specific heat jump for hole concentrations less than optimal doping ($\delta \gtrsim 0.1$) seen in Fig. 2. $\gamma_{\rm el} (= \partial S_{\rm el}/\partial T)$ was calculated from the free-electron entropy density, using Eq. (9). The temperature dependence of the superconducting order parameter in the presence of the normal-state pseudogap was determined using the BCS equation in a manner similar to that described previously.[41] The resultant calculated values of $\gamma_{\rm el}(T)$ are shown in Fig. 9(a) where the arrow indicates decreasing E_g (increasing hole concentration). This model accounts for the general trends in the overall T dependence of $\gamma_{\rm el}$ as well as the decrease in condensate energy and superfluid density at low temperatures with increasing E_g (decreasing hole concentration).

As noted above, ARPES studies have confirmed the existence of the pseudogap and the anisotropy of the normal-state gap. Analysis of the leading edge of the ARPES spectra for underdoped $Bi_2Sr_2CaCu_2O_8$ shows a gap that appears to smoothly evolve from the superconducting gap at low T falling linearly to zero magnitude at some higher temperature, let us say, T^*, well above T_c.[8,49,50] This has been taken as confirmation that the pseudogap corresponds to short-range pairing correlations that set in at a mean-field temperature T^*, without developing long-range phase coherence until the lower temperature, T_c. However, there is no satisfactory model for the spectral line shape and the leading-edge analysis is oversimplified. This is highlighted by the fact that the concluded behavior is inconsistent with the thermodynamics of the problem. The second-order transition at T_c requires a positive discontinuity in the slope $d\Delta/dT$ at T_c, leading to the observed discontinuity in $\gamma_{\rm el}$, which is not present in the gap data inferred from the ARPES results. Figure 9(b) shows the calculated T dependence of $\gamma_{\rm el}$ using $E_g = E_{g0}(1 - T/T^*)$ and a d-wave order parameter below T_c. It

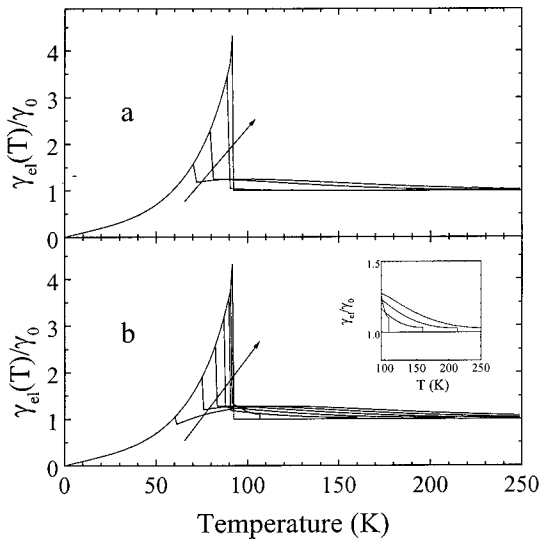

FIG. 9. (a) The temperature dependence of the normalized γ_{el} expected from the Fermi surface evolution model described in the text. The arrow indicates decreasing E_g (increasing hole concentration). (b) Plot of $\gamma_{el}(T)$ expected from the model described in the text and an E_g that is linearly dependent on temperature. The arrow indicates decreasing E_g (increasing hole concentration). Insert: Expanded plot of (b).

can be seen that a linearly dependent $\Delta(T)$ above T_c leads to a strong T dependence of γ_{el} not present in the data, and the fall to zero of $\Delta(T)$ at $T=T^*$ leads to a discontinuity in γ_{el} at T^* also not present in the data. This calculated behavior is illustrated in detail by the enlargement shown in the insert to Fig. 9(b). Such behavior is not evident in the experimental data of Fig. 2. Again, these considerations are largely independent of the specific model adopted. We may add that detailed NMR and heat capacity studies show the pseudogap and superconductivity to be independent and competing to low temperatures,[42] an observation strongly confirmed by the absence of an isotope effect in the pseudogap energy and the concurrent presence of a superconducting isotope effect.[51] Finally, we recall that E_g progresses with underdoping to a magnitude of the order of $J \gg \Delta_0$. In light of these observations it is difficult to sustain the view that the pseudogap is some form of precursor superconductivity setting in at a mean-field transition temperature lying well above T_c.

Finally, we distinguish between $T_U \sim E_g/k_B$ and the temperature T_p, at which a maximum in χ_s occurs. In our model we assume a flat underlying DOS. In fact there is strong evidence that a sharp van-Hove-singularity-like peak in the DOS crosses the Fermi level in the heavily overdoped region near the superconductor/metal transition.[52–54] This quite naturally leads to a broad maximum in χ_s with a very high value of T_p in the underdoped region that progresses to low temperature and sharpens in the overdoped region. As such, T_p, also does not represent a crossover or onset temperature.

CONCLUSION

In conclusion, we find no evidence for well-defined onset temperatures, T_L and T_U, in NMR Knight-shift, heat capacity, or resistivity data. The T_L observed in NMR $1/^{63}T_1T$ measurements is an artefact of the convolution of the $1/T$ Curie term with the typical pseudogap temperature dependence of $1/^{63}T_1 \propto \chi_s$ and is illustrated by the fact that $^{63}T_1T$ multiplied by the NMR Knight shift is perfectly linear and featureless at T_L. The absence of a T_L and T_U in the NMR Knight-shift, heat capacity, or resistivity data can be accounted for in the NAFL model by including a dynamic spin susceptibility that is directly proportional to $\chi_s(T)$ as originally proposed by Millis, Monien, and Pines. These observations require a reappraisal of some of the current complex models for the high-temperature superconducting phase diagram that invoke several crossover temperatures.

ACKNOWLEDGMENTS

Funding for this work was provided by the New Zealand Foundation for Research Science and Technology (G.V.M.W), the Royal Society of New Zealand (J.L.T), and the U.K. Engineering and Physical Sciences Research Council (J.W.L).

[1] J. W. Loram, K. A. Mirza, J. R. Cooper, and W. Y. Liang, J. Supercond. **7**, 243 (1994).
[2] J. R. Cooper and J. W. Loram, J. Phys. I **6**, 1 (1996).
[3] J. L. Tallon *et al.*, Phys. Rev. Lett. **75**, 4114 (1995).
[4] G. V. M. Williams, J. L. Tallon, R. Michalak, and R. Dupree, Phys. Rev. B **54**, 6909 (1996).
[5] G. V. M. Williams *et al.*, Phys. Rev. Lett. **78**, 721 (1997).
[6] A. Janossy, T. Feher, G. Oszlanyi, and G. V. M. Williams, Phys. Rev. Lett. **79**, 2726 (1997).
[7] A. G. Loeser *et al.*, Science **273**, 325 (1996).
[8] H. Ding *et al.*, Nature (London) **382**, 51 (1996).
[9] J. W. Loram *et al.*, *Advances in Superconductivity VII* (Springer-Verlag, Tokyo, 1995), p. 75.
[10] V. J. Emery and S. A. Kivelson, Nature (London) **374**, 434 (1995).
[11] A. S. Alexandrov, V. V. Kabanov, and N. F. Mott, Phys. Rev. Lett. **77**, 4796 (1996).
[12] H. Fukuyama, H. Kohno, and T. Tanamoto, J. Low Temp. Phys. **95**, 309 (1994).
[13] P. A. Lee and X. G. Wen, Phys. Rev. Lett. **76**, 503 (1996).
[14] D. Pines, Physica C **282-287**, 273 (1997).
[15] T. Dahm, D. Manske, and L. Tewordt, Phys. Rev. B **56**, 11 419 (1997).
[16] U. Löw, V. J. Emery, K. Fabricius, and S. A. Kivelson, Phys. Rev. Lett. **72**, 1918 (1994).
[17] S.-C. Zhang, Science **275**, 1089 (1997).
[18] A. J. Millis, L. B. Ioffe, and H. Monien, J. Phys. Chem. Solids **56**, 1641 (1995).
[19] D. Pines, Z. Phys. B **103**, 129 (1997).
[20] I. Tomeno *et al.*, Phys. Rev. B **49**, 15 327 (1994).
[21] J. Yasuoka, Physica C **282-287**, 199 (1997).
[22] A. Chubukov, D. Pines, and B. Stojkovic, J. Phys.: Condens. Matter **8**, 1 (1996).
[23] V. Barzykin and D. Pines, Phys. Rev. B **52**, 13 585 (1995).

[24] J. Rossat-Mignot, L. P. Regnault, and C. Vettier, Physica B **180-181**, 383 (1992); L. P. Regnault *et al.*, Physica C **235-240**, 59 (1995).
[25] Ch. Renner *et al.*, Phys. Rev. Lett. **80**, 149 (1998).
[26] R. L. Corey *et al.*, Phys. Rev. B **53**, 5907 (1996).
[27] N. J. Curro, T. Imai, C. P. Slichter, and B. Dabrowski, Phys. Rev. B **56**, 877 (1997).
[28] A. Keren, H. Alloul, P. Mendels, and Y. Yoshinari, Phys. Rev. Lett. **78**, 3547 (1997).
[29] T. Oto, K. Takenaka, and S. Uchida, Phys. Rev. Lett. **70**, 3995 (1993); B. Battlog *et al.*, Physica C **235-240**, 130 (1994).
[30] M. Reedyke *et al.*, Phys. Rev. B **56**, 9129 (1997).
[31] R. Nemetschek *et al.*, Phys. Rev. Lett. **78**, 4837 (1997).
[32] J. M. Harris *et al.*, Phys. Rev. B **54**, 15 665 (1996).
[33] A. J. Millis, H. Monien, and D. Pines, Phys. Rev. B **42**, 167 (1990).
[34] S. D. Obertelli, J. R. Cooper, and J. L. Tallon, Phys. Rev. B **46**, 14 928 (1992).
[35] M. R. Presland *et al.*, Physica C **176**, 95 (1991).
[36] N. E. Hussey *et al.*, Phys. Rev. B **56**, 11 423 (1997).
[37] J. W. Loram *et al.*, Physica C **235-240**, 134 (1994); J. W. Loram and K. A. Mirza, in *Electronic Properties of High Temperature Superconductors*, edited by H. Kuzmany, M. Mehring, and J. Fink (Springer-Verlag, New York, 1990).
[38] M. Takigawa *et al.*, Phys. Rev. B **43**, 247 (1991).
[39] F. Mila and T. M. Rice, Physica C **157**, 561 (1989).
[40] J. W. Loram *et al.*, Physica C **282-287**, 1405 (1997).
[41] J. L. Tallon, G. V. M Williams, N. E. Flower, and C. Bernhard, Physica C **282-287**, 236 (1997).
[42] J. L. Tallon, J. W. Loram, and G. V. M. Williams (unpublished).
[43] J. L. Tallon, C. Bernhard, G. V. M. Williams, and J. W. Loram, Phys. Rev. Lett. **79**, 5294 (1997).
[44] G. V. M. Williams, E. M. Haines, and J. L. Tallon, Phys. Rev. B **57**, 146 (1998).
[45] For a review, see, R. S. Markiewicz, J. Phys. Chem. Solids **58**, 1179 (1997).
[46] J. Wheatley, Physica C **207**, 102 (1993).
[47] Z.-X. Shen and J. R. Schrieffer, Phys. Rev. Lett. **78**, 1771 (1997).
[48] M. R. Norman, M. Randeria, H. Ding, and J. C. Campuzano (unpublished).
[49] M. R. Norman, H. Ding, and D. G. Hinks, Nature **392**, 157 (1998).
[50] J. M. Harris *et al.*, Phys. Rev. B **54**, 15 665 (1996).
[51] G. V. M. Williams *et al.*, Phys. Rev. Lett. **80**, 377 (1998).
[52] J. W. Loram *et al.*, *Proceedings of the 10th Anniversary HTS Workshop on Physics Materials and Applications* (World Scientific, Singapore, 1996), p. 341.
[53] G. V. M. Williams, J. L. Tallon, R. Michalak, and R. Dupree, Phys. Rev. B **57**, 8696 (1998).
[54] A. Ino *et al.*, Phys. Rev. Lett. **81**, 2124 (1998).